IEEE Access
Multidisciplinary | Rapid Review | Open Access Journal

Received 8 December 2022, accepted 30 December 2022, date of publication 10 January 2023, date of current version 17 January 2023.
Digital Object Identifier 10.1109/ACCESS.2023.3235822

RESEARCH ARTICLE

A Circularly Polarized Parallel Plate Waveguide Lens-Like Multiple-Beam Linear Array Antenna for Satcom Applications

NICOLA BARTOLOMEI[1], DARWIN BLANCO[1], FRANÇOIS DOUCET[1], ETIENNE GIRARD[2], HERVÉ LEGAY[2], NELSON J. G. FONSECA[3], (Senior Member, IEEE), RONAN SAULEAU[1], (Fellow, IEEE), AND MAURO ETTORRE[1], (Fellow, IEEE)
[1]CNRS, Institut d'Electronique et des Technologies du numéRique (IETR)—UMR 6164, University of Rennes 1, 35000 Rennes, France
[2]Thales Alenia Space, 31100 Toulouse, France
[3]Antenna and Sub-Millimeter Waves Section, European Space Agency, 2200 AG Noordwijk, The Netherlands

Corresponding author: Nicola Bartolomei (nicola.bartolomei@wave-up.it)

This work was supported in part by the Thales Group through the KTD action France; in part by the European Union through the European Regional Development Fund (ERDF); in part by the Ministry of Higher Education and Research; in part by the Région Bretagne; in part by the Conseil Départemantal des Côtes d'Armor; and in part by the Conseil Départemental d'Ille et Vilaine, through the CPER Projects 2015–2020 MATECOM and SOPHIE/STIC and Ondes.

ABSTRACT This work presents a full metal circularly-polarized lens-like antenna for Satcom applications at Ka-band. The antenna is composed of two continuous parallel plate waveguide (PPW) quasi-optical beamformers (QOBF), feeding an array of septum polarizers to generate circular polarization. The QOBFs operate over a wide band and provide a multi-beam coverage over a large field of view in the azimuthal plane, while maintaining a relatively simple mechanical design. The array of septum polarizers is based on a stepped profile to generate circular polarization with a good polarization purity in the uplink of Ka-band (27 - 31 GHz). The antenna is fully realized in aluminium. The antenna system provides 14 beams with alternating right/left handed circular polarization (RHCP/LHCP) with an axial ratio (AR) below 3 Db over an angular range of $\pm 19^\circ$ in the uplink of Ka-Band. The maximum gain in the azimuthal plane at 30 GHz is about 21 dB over the whole angular range, with a scan loss lower than 1.5 dB. The antenna efficiency is better than 78% for all beams in the operative band.

INDEX TERMS Beamformers, circular polarization, parallel plate waveguides, satcom applications, septum polarizer.

I. INTRODUCTION

The increasing demand for high performance and low-cost multiple-beam antennas in the millimeter-wave range for satellite communications has driven the development of novel solutions. Multiple-beam antennas have been often realized using beamforming networks (BFN) based on Blass [1], [2], Nolen [3], [4], or Butler [5], [6], matrices which combine several elementary components (e.g., couplers and phase shifters) to provide aperture sharing and beam switching capabilities. However, such BFNs are complex and often narrow band as they generally rely on a phase shifting approach rather than a true-time delay approach [33]. For broadband applications it is usually preferred to use QOBFs such as pillbox reflectors [13], Luneburg lenses [7], [8], [37] and constrained lenses, also referred to as bootlace lenses [12], Ruze [9], Rotman [10]. These lenses exhibit multiple true focal points (except for the pillbox system), thus resulting in low phase aberrations over a wide scanning range. However, the constrained lens design is based on discrete transmission lines connecting the outer lens contour and the radiating aperture. The discretization of the aperture entails some limitations highly dependent on the transmission line technology used. The original design by Rotman and

The associate editor coordinating the review of this manuscript and approving it for publication was Hussein Attia.

Turner [11] is very wideband thanks to the use of coaxial transmission lines which allows a very fine discretization of the aperture, but with the drawback of integration complexity.

The QOBF exhibits wideband characteristic, thanks to the continuous PPW lens beamformer, with less complexity and usually with more compactness with respect to common Rotman lens designs.

In literature there are alternative planar designs in printed technology using either microstrip or substrate integrated waveguide (SIW) [19], [20]. These structures are simpler to manufacture and low profile, but they have in general a more coarse discretization (typically around half-a-wavelength at the operating frequency) leading to a limitation of the upper frequency of operation due to the appearance of grating lobes in the scanning range. These solutions also tend to have higher losses due to the use of dielectric materials and higher mismatch losses between the PPW section and the transmission lines for large scanning angles. Folded and modulated geodesic lenses are discussed in [32], [34], and [35]. These antennas present wide frequency band and large scanning range, but they generate beams with a single linear polarization. A continuous PPW lens beamformer providing wide scanning performance, wide bandwidth and relatively easy mechanical design was introduced in [15]. A design procedure using a bifocal constrained lens equivalence was proposed and experimentally validated in [14], [16], and [17]. The beamformer in [17] converts the cylindrical waves launched by a feeding horn inside the PPW to nearly plane waves by means of a ridge introduced within the PPW structure and operating as a delay lens. The proposed lens is defined by its inner contour (Σ_1) and ridge height profile (h_w). Both are optimized to minimize phase aberrations for extreme offset feeds defined at angular positions $\pm\alpha$ and generating beams pointing in diametrically opposite directions. The other feeds are defined along an optimized focal curve, as for a Rotman lens design [10].

This system exhibits very good performance in terms of bandwidth and scanning capability. However this antenna radiates a linearly-polarized field while circular polarization (CP) is generally preferred for broadband SatCom applications. To overcome this limitation the QOBF has been used together with a wideband curved polarizing reflector [21]. Reflectors can offer very attractive performance in terms of axial ratio purity; however they present a drawback in terms of compactness. A more compact solution consists in using a stepped septum polarizer in a square waveguide. Such a component consists of a three port device formed by a square waveguide with a septum located in the middle creating two rectangular waveguides at the other end of the device. By exciting one of the two rectangular waveguides with its fundamental Transverse Electric mode (TE_{10}), the energy is partially transferred by the septum to the orthogonal TE_{01} mode of the square waveguide. A right-handed (RHCP) or left-handed (LHCP) circularly-polarized field is generated at the output of the polarizer depending on the feeding rectangular waveguide. The waveguide polarizing septum (WPS) has been extensively used and was first introduced with a sharp profile in [23]. The shape of the septum was successively improved; a notch septum was presented in [24], which allows a very compact design at the expense of a reduced bandwidth with respect to [25] and [26]. However, those solutions require an additional dielectric slab for phase adjustment, which may be undesirable for space applications. A stepped septum polarizer without any additional phase adjustment was proposed in [27]. In [28] the thickness of the septum was taken in account, showing its impact on the bandwidth and axial ratio and in [29] a computer-aided optimization technique was described. In more recent works, stepped septum polarizers are used as stand-alone devices to provide circularly polarized sources for various applications and frequency bandwidth. In [43], a septum polarizer is used to feed a quad-ridged horn antenna covering a band of 40% in X-band. In [46] a compact stepped-thickness septum polarizer with a square-to-circular transition, operating in the X-band 7.25 − 8.60 GHz, is designed with 3 steps. In [41] a wide band, up to 46% septum polarizer is achieved by using a triangular common port instead of a square one, while in [42] the authors provide a design technique to reduce the impact of misalignment errors for the split-block manufacturing technique. In [47], [48], and [49] stepped septum polarizers has been designed for sub-millimeter wave applications (above 100 GHz) showing good performance. Those works all presents stepped septums polarizers as a stand-alone device. The first attempt to introduce a septum polarizer in a quasi-optical system is presented in [36], where a septum polarizer is directly realized in a parallel plate waveguide. Although it may be a simpler solution, this antenna has a dispersive response because of the use of PPW quasi Transverse Electromagnetic (q-TEM) and TE_{01} modes to obtain circular polarization, which have a different wave's impedance and a different phase velocity. In this paper we propose the design of a full-metal array of septum polarizers [50], realized in electrical discharge machining (EDM) technique, which has been optimized and integrated with a pair of PPW QOBF to obtain a multi-beam antenna capable of generating circularly polarized beams in the the Ka-band uplink for Satcom applications. To the best of our knowledge this is the first design of a circularly polarized quasi-optical multi-beam antenna in a fully integrated system, validated by a measured prototype.

This paper is organized as follows. The antenna architecture and the design guidelines for each part of the antenna are presented in Sec. II. Manufacturing and measured results are discussed in Sec. III. Conclusions are drawn in Sec. IV.

II. PROPOSED ANTENNA SYSTEM

The proposed antenna system is designed to provide 14 circularly polarized beams covering a $\pm 19°$ scanning range with a step of about 3° and alternating RHCP and LHCP between adjacent beams for higher isolation, as depicted in Fig. 1.

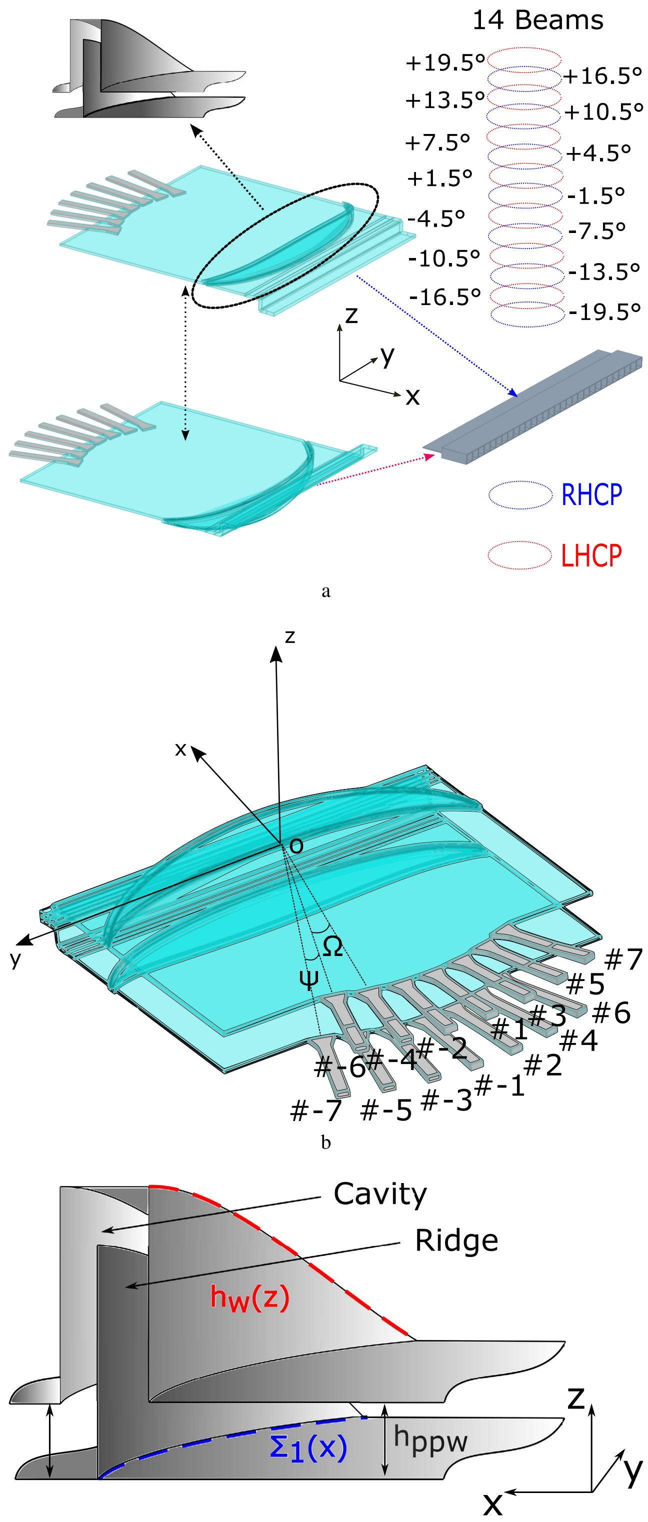

FIGURE 1. **Proposed antenna system: (a) 14 beams alternating RCHP and LHCP are generated in xy-plane or azimuthal plane, (b) The upper QOBF generates 7 RCHP beams while the lower 7 LHCP beams, (c) Cross sectional detail of the shaped ridge and cavity profile.**

An array of septum polarizers is therefore used together with two identical QOBFs mirrored with respect to the beamforming plane. The septum array polarizer is connected to the QOBFs through a transition able to convert the q-TEM mode, supported by the PPW, into the fundamental TE_{10} supported by the input rectangular waveguides of the septum polarizers. Each QOBF can generate seven linearly polarized beams, according to the selected feeding horn. The feeding horns, positioned along the focal curve of the PPW lens, are angularly spaced of about $\Omega = 6°$ and shifted of $\psi = 3°$ with respect to the other QOBF's feeds as depicted in Fig. 1b. This particular arrangement, similar to the one also described in [18], allows to have alternate RHCP/LHCP between two adjacent beams, inasmuch they are generated by different PPWs, and it allows also an adequate beam cross-over level (sightly over 3 dB below the peak directivity) while preserving enough space between two consecutive horns. The horns were designed to provide an adequate edge tapering (about -10 dB considering broadside beam) over the lens contour (Sec. II-A). The edge tapering is fundamental to minimize the effect of the side walls, which may increase the phase aberration and SLL.

A. PPW CONTINUOUS LENS-LIKE BEAMFORMER

The QOBFs have a design similar to the one described in [18], and optimized to achieve a maximum scanning angle on the azimuthal plane of $\phi_s = \pm 31.5°$. In particular a polynomial shaped delay lens profile (inner lens contour Σ_1 and ridge height profile h_w as shown in Fig. 1c) is defined as follow:

$$\Sigma_1(x) = \sum_{k=1}^{n} p_k y^k \tag{1}$$

$$h_w(z) = \sum_{k=1}^{n} q_k y^y - \min\left(\sum_{k=1}^{n} q_k y^k\right) \tag{2}$$

where x, y, z are normalized to the focal distance f, p_k and q_k are the k^{th} order coefficients with $1 \leq k \leq n$, n the maximum degree of the polynomial function.

Using the Geometrical Optics (GO) continuous lens model pattern optimization detailed in [18] two identical QOBFs have been designed. The optimized polynomial profile coefficients are shown in table 1, while the maximum height of the ridge $h_w(z_{\max}) = 21$ mm.

The thickness of the ridge is $|\Sigma_2 - \Sigma_1| = 2$ mm, where Σ_2 is the outer contour of the ridge and it is obtained by a translation of the inner contour Σ_1 along the x-axis (Fig. 1c). The choice of the thickness is the minimum achievable by milling machining without potentially bending the blade. The PPW's height is $h_{\text{ppw}} = 2$ mm, which guarantee the propagation of the fundamental q-TEM of the PPW structure over the whole operative band. The lens diameter is $D = 20\lambda_0$ at the operative frequency $f_0 = 30$ GHz, and the focal distance is $F = 0.7D$.

Each QOBF is fed by one of the 7 horns disposed along a circular focal curve centered in O and traced between the two focal points F_1 and F_2 as shown in Fig. 2b, so that one QOBF covers the angular range between $-16.5°$ and $19.5°$ and the other from $-19.5°$ and $16.5°$. Both focal points are

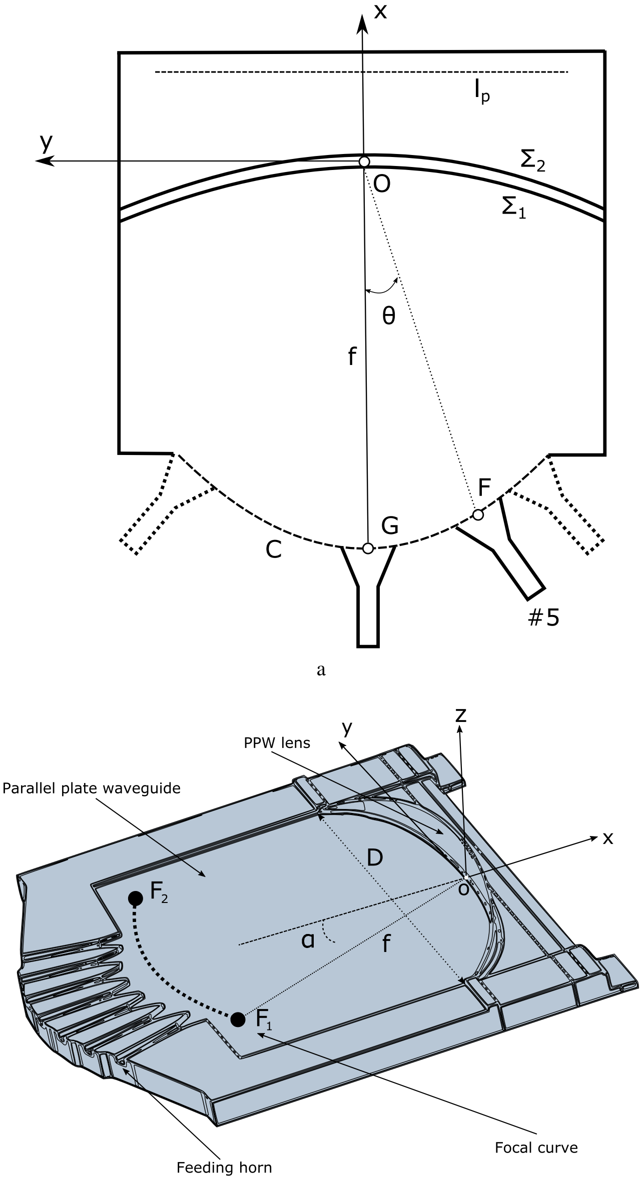

FIGURE 2. Parallel plate lens-like structure: (a) 2D sketch of the QOBF, (b) 3D view of one of the two identical continuous PPW lens-like beamformers.

TABLE 1. Optimized polynomial profile coefficients with the GO tool in [18] and a polynomial maximum order set to $n = 10$.

p_1	p_2	p_3	p_4	p_5	p_6
-0.2167	-0.7468	-0.165	-0.0901	-0.2462	0.0131
q_1	q_2	q_3	q_4	q_5	q_6
-0.5267	-0.0476	0.0381	0.0613	-0.2364	0.121

symmetrical with respect to the x-axis, and they are defined by their angular positions $\alpha = \pm 31.5°$. The horns launch a cylindrical wave inside the PPW which is converted in a nearly plane wave feeding in turn one of the two ports of the septum polarizers linear array. They have an aperture size $a_{feed} = 14$ mm, about $1.5\lambda_0$ at f_0, and height of $h_{\text{ppw}} = 2$ mm.

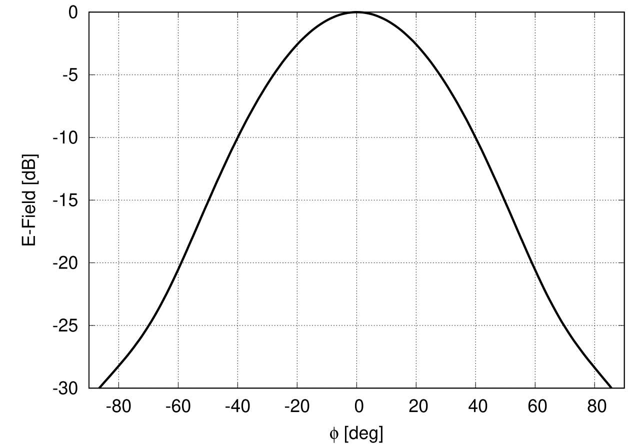

FIGURE 3. Normalized field amplitude at f_0 launched inside the PPW, calculated along a line l_p posed at the output of the QOBF.

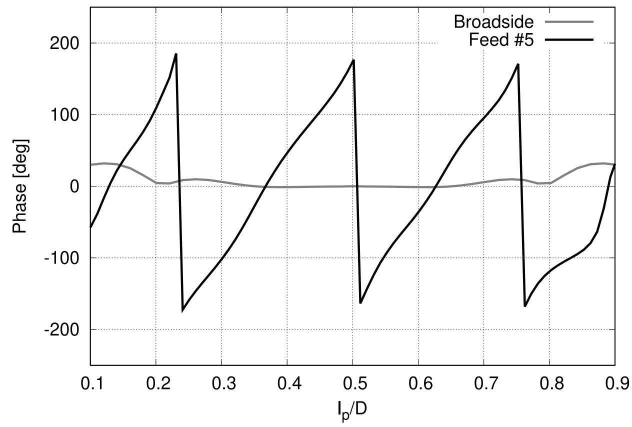

FIGURE 4. Phase distribution calculated along a line l_p posed at the output of the QOBF.

Such aperture size is chosen to achieve an edge taper of about -10 dB considering a focal-to-length ratio F/D = 0.7. Fig.3 shows the normalized field amplitude launched inside the PPW by an horn at the center G of the focal curve C as sketched in Fig. 2. The cylindrical-to-planar wave front conversion achieved by the QOBF is shown in Fig. 4: the phase distribution along a line $l_p = 0.7$D long (corresponding to -10 dB field tapering) at the output of the QOBF is depicted for a feeding horn at the center G of the focal curve C and when feed #5 (Fig. 2) is active. The maximum phase distortion with respect to an ideal TEM-mode phase front is about $\pm 25°$, corrisponding to a phase rotation of less than 0.07 wavelengths at the center frequency $f_0 = 30.0$ GHz. The horns are fed by standard WR28 waveguides and thus a transition to coaxial line is used in measurements.

B. SEPTUM LINEAR ARRAY POLARIZER

The septum array polarizer has been first designed as a stand-alone device. The circular polarization generation can be easily explained considering two cases for the excitation of the two input rectangular waveguides. When the two input

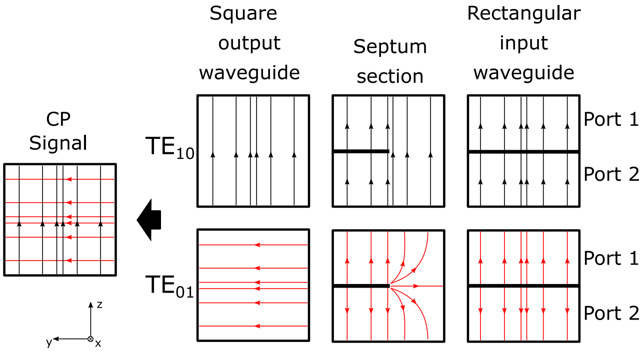

FIGURE 5. Stepped septum polarizer circular polarization generation: graphical explanation.

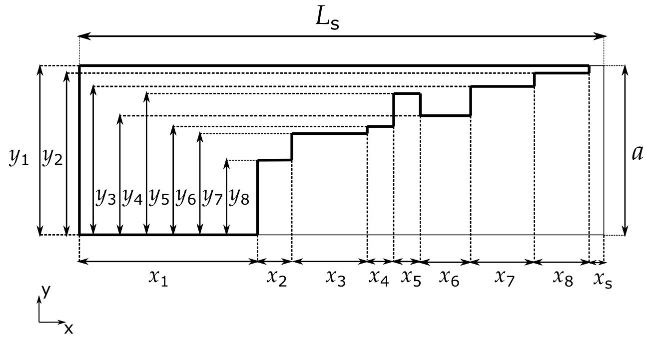

FIGURE 7. Optimized profile of the stepped septum polarizer (the dimensions, in mm, are listed in Table 2).

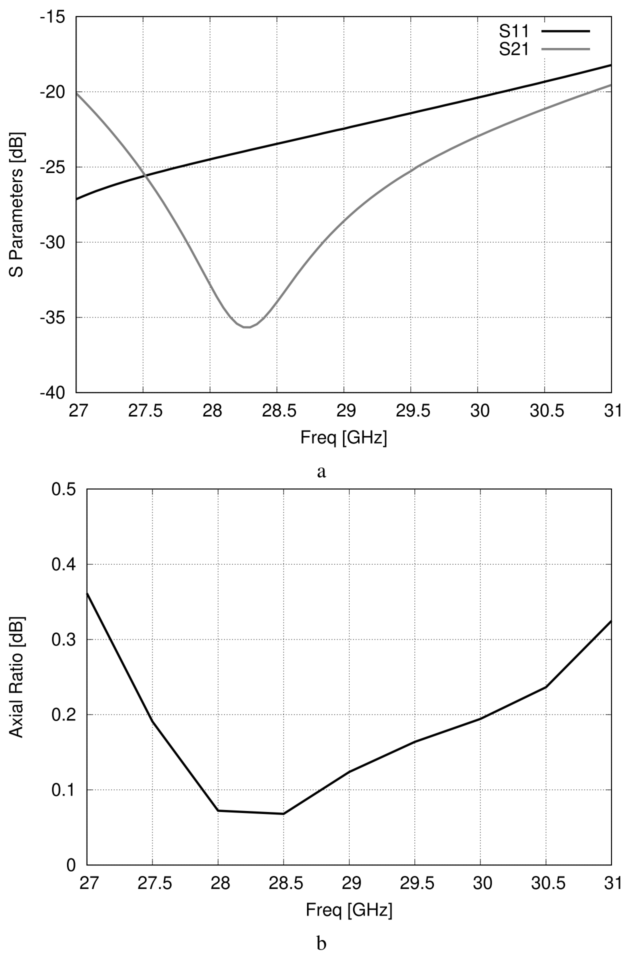

FIGURE 6. Performances of the optimized septum polarizer: (a) Reflection coefficient and isolation between the input ports, (b) Axial ratio.

ports are excited in phase, the field passes through the septum section almost unperturbed, as the electric currents circulate in opposite directions on either side of the septum surface, and the fundamental TE_{10} is launched at the output port. When the input ports are excited out of phase, the electric current flows in the same direction on either side of the septum surface, so that the septum side edge becomes a charge accumulation point, supporting a field component orthogonal with respect to the input one, and the fundamental TE_{10} mode is launched at the output port. Moreover E_y component, propagating along a stepped septum, has a slower phase velocity with respect to E_z component. The stepped profile introduces a spatially varying height ridge effect, which lowers the cutoff frequency controlling the delay. The operation of the septum polarizer is graphically reppresented in Fig. 5 for clarity. The profile has been optimized considering a three ports device: the goal is minimizing the input matching ratio while maximizing the transmission to the common port forcing the delay of the E_y component with respect to E_z to be about $\pm 90°$ over the operating frequency band. An approximated, but still accurate enough formula, is provided in [30] The general approximated formula for axial ratio is given by:

$$\mathrm{AR}|_{\mathrm{dB}} = \left[A_e^2 + (0.15)^2 \cdot (\phi_e + \beta_e)^2\right]^{\frac{1}{2}} \tag{3}$$

assuming the complex voltage excitation for the two components E_z and E_y as:

$$\frac{E_z}{E_y} = Ae^{i\phi} \tag{4}$$

The error coefficients in [30] are defined as follows:

$$A_e|_{\mathrm{dB}} = 20log_{10}\,(A) \tag{5}$$
$$\phi_e|_{\mathrm{deg}} = 90 - |\phi| \tag{6}$$
$$\beta_e|_{\mathrm{deg}} = 90 - \beta \tag{7}$$

Equation (3) takes in account all the possible sources of errors for two perfectly linear sources generating circular polarization: amplitude and phase error (A_e, ϕ_e), accounting for unequal amplitude of the field components and deviation from nominal quadrature-phase difference respectively, and orthogonality error (β_e), accounting for slightly non-orthogonal modal field distributions at the radiating aperture. The thickness of the septum t is set to 0.5 mm, which is sightly higher than standard values used at these frequencies [22], but necessary to guarantee the feasibility through EDM. This particular technique allows to manufacture the septum linear array polarizer in a monolithics metal block, avoiding possible electrical contact problems in multiple

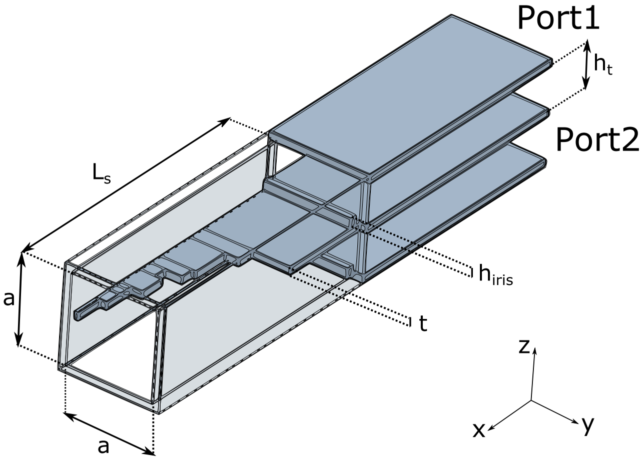

FIGURE 8. Unit-cell of the stepped septum polarizer.

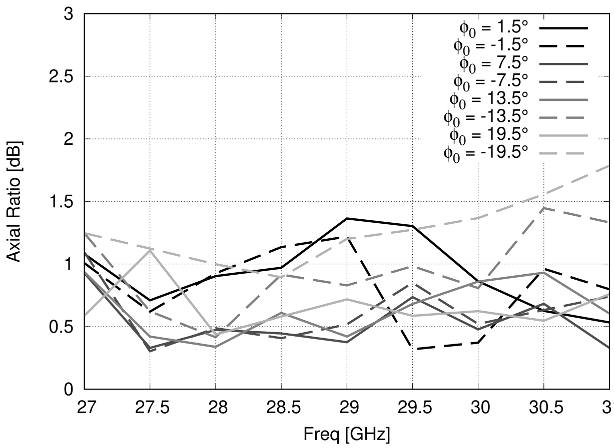

FIGURE 9. Scanning performance along the azimuthal plane (constant $\theta = 90°$ with respect to the coordinate system in Fig. 8) of the optimized septum polarizer in a periodic environment.

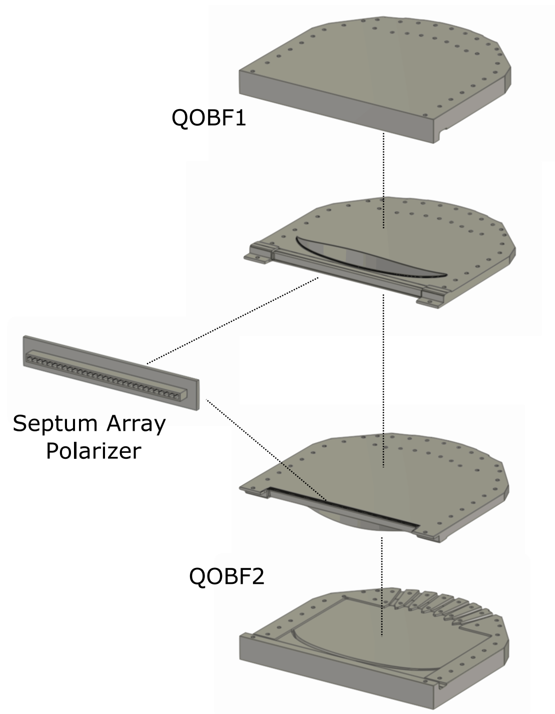

FIGURE 10. Exploded view of the antenna: four metal blocks are screwed together and the septum array polarizer is fixed between the two QOBFs.

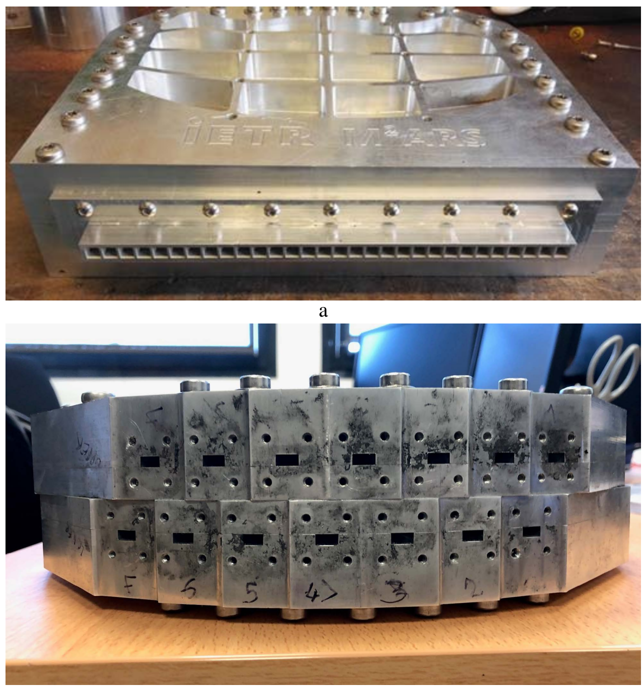

FIGURE 11. Manufactured prototype: (a) View from the array of septum polarizers, (b) View from the input ports.

blocks realizations. The sizes of the square waveguide width and height are set to $a = 6.35$ mm with a walls' thickness of $t = 0.5$ mm. The input ports height is $h_t = 2.925$ mm, while the length L_s of the septum middle plate is an optimization parameter. The size of the square waveguide fixes the periodicity of the septum array to $p = 7.35$ mm, which is about $0.7\lambda_0$ at $f_0 = 30$ GHz. Even if the QOBF is capable of wide scanning, namely $\theta_s = \pm 31.5°$, the periodicity of the septum array limits the scanning to $\theta_s = \pm 20°$, due to the generation of grating lobes for larger angles. A full-wave optimization based on a global algorithm is thus performed by considering two waveguide ports feeding a septum made of seven steps. Designs of conventional septum polarizers have been reported with less steps while still covering a similar fractional bandwidth. However, the specific operation of the proposed polarizer, transitioning from a PPW to a rectangular waveguide was found to require more degrees of freedom to guarantee good performance of axial ratio and input matching as the incident angle increase from broadside. The goal function takes in account the scattering parameters of the device and the radiated fields: each septum's step is sized in order to maximimize the matching for all the three ports of the polarizer (the two rectangular waveguide input ports and the

TABLE 2. Dimensions in mm of the stepped septum polarizer.

L_s	x_1	x_2	x_3	x_4	x_5	x_6	x_7	x_8
19.67	6.68	1.29	2.83	0.99	1.00	1.89	2.39	2.05
a	y_1	y_2	y_3	y_4	y_5	y_6	y_7	y_8
6.35	6.35	3.55	2.56	2.29	1.05	1.57	0.79	0.29

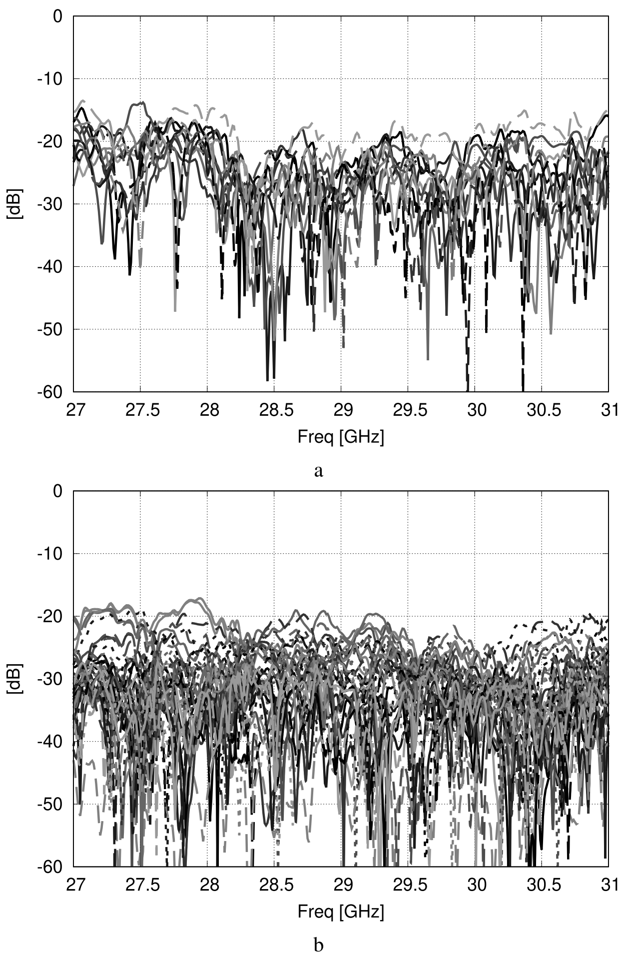

FIGURE 12. Scattering parameters (*S*-matrix) of the measured prototype: (a) Reflection coefficient for each input port, (b) Mutual coupling between the feeding ports.

square waveguide output port) and maximize the isolation while minimizing the axial ratio cost function (3), over the operative uplink Ka-band (27 − 31 GHz). In Fig. 6a the performances of the designed septum polarized are shown: the reflection coefficient and the isolation between the input ports are both below −18 dB (Fig. 6). The axial ratio shows an excellent circularly polarization purity, below 0.4 dB over the operative band (Fig. 6b).

Then the single element of the array, fed by two PPWs, has been simulated and optimized in a periodic environment as in Fig. 8, to study the scanning performances. The transition between the PPWs and the rectangular input waveguides of the septum polarizer is obtained by inserting in each input waveguide a capacitive iris of height h_{iris} = 0.69 mm and thickness t = 0.5 mm, posed at z_{iris} = 0.44 mm from

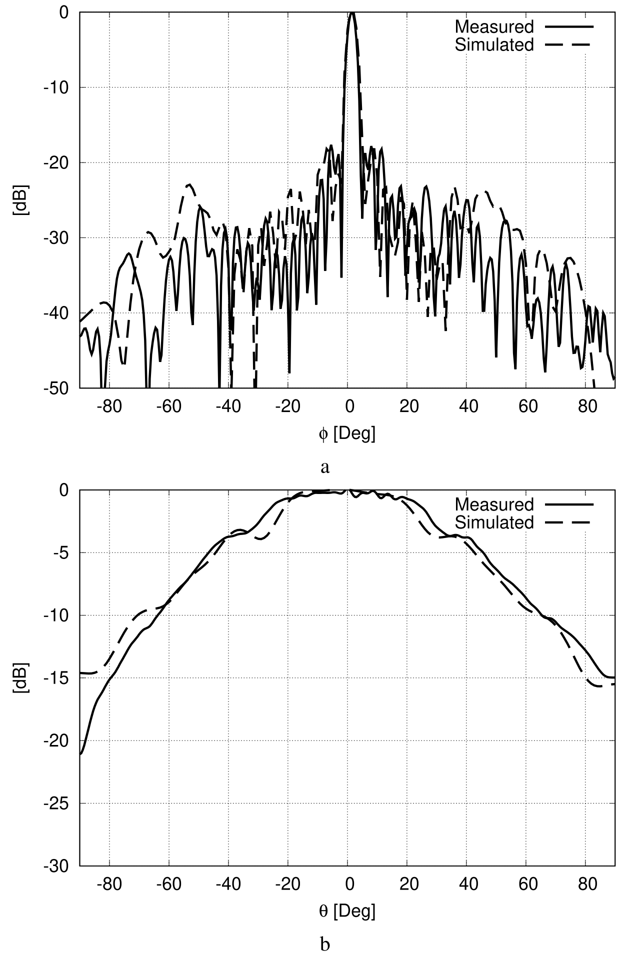

FIGURE 13. Normalized directivity patterns on the principal planes for the central beam pointing at $\phi_0 = 1.5°$ at 29 GHz: (a) Azimuthal plane (constant $\theta = 90°$), (b) Elevation plane (constant $\phi = \phi_0$).

the discontinuity. The circular polarization purity can be estimated through the computation of the far fields considering the cross-polar component rejection as defined in [44]. Or equivalently it can be expressed in terms of axial ratio, defined as the ratio of the lengths of the major and minor axes of the polarization ellipse of the radiated field defined as in [45]:

$$\mathrm{AR} = \frac{|E_z|^2 + |E_y|^2 + \sqrt{\gamma}}{|E_z|^2 + |E_y|^2 - \sqrt{\gamma}} \tag{8}$$

where the parameter γ is given by:

$$\gamma = |E_z|^4 + |E_y|^4 + 2|E_z|^2|E_y|^2 \cos\left[2\left(\angle E_z - \angle E_y\right)\right] \tag{9}$$

The optimized width and length of each step, x_n and y_n respectively, are shown in table 2, the final length of the blade is 19.12 mm, while the total length of the square waveguide is L_s = 19.67 mm. A small section of x_s = 0.55 mm right after the septum is required to improve the matching with free space. Fig. 9 shows the axial ratio, which is sightly degraded with respect to the performance of the stand-alone septum polarizer, due to the strong coupling between the array

TABLE 3. Comparison of the proposed antenna with previously published works on dual circularly polarized antennas in Ka-band.

Ref.	N. Elements	Tech.	Scan. Range	BW [%]	Gain [dBi]	Avg. Eff. [%]
[39]	1x4	SIW	±38°	22.5*	10.4-12.8	50
[40]	16x16	Full Metal	Fix. Beam	16	31.4-32.8	60
[38]	8x8	Full Metal	Fix. Beam	4.96	27-27.8	75
This work	1x32	Full Metal	±19.5°	8.85*	20-22	85

V*Bandwidth considered in the scanning range.

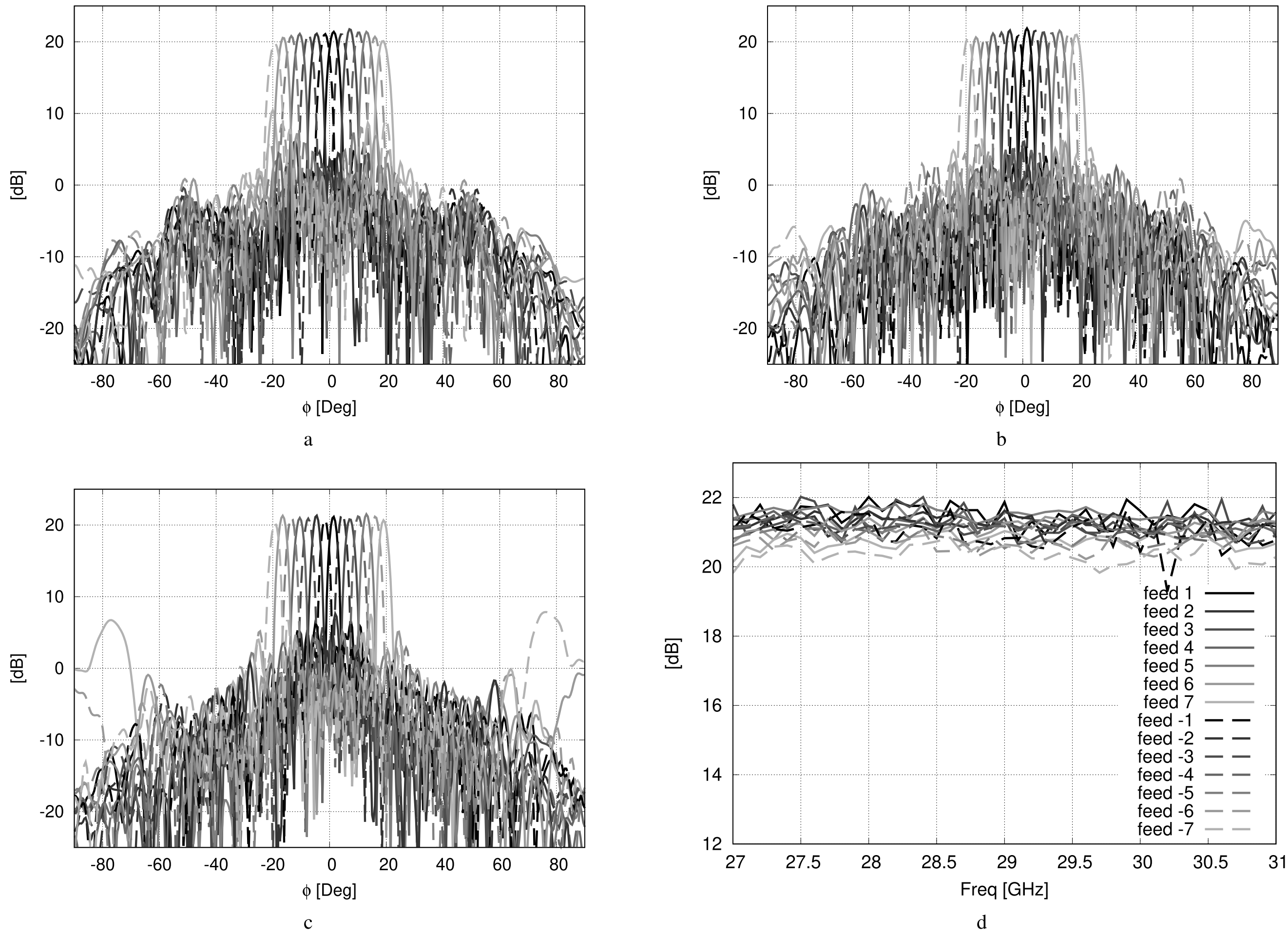

FIGURE 14. Measured Gain along the azimuthal plane (Co-polar components): (a) Freq = 27 GHz, (b) Freq = 29 GHz, (c) Freq = 31 GHz, (d) measured realized gain for all the ports over frequency.

elements. However a good purity of circular polarization is maintained, namely below 2 dB over the operative band for the whole scan range. It is also worth noticing that the asymmetry in the performance is due to the asymmetric design of the septum polarizer.

C. FINAL ANTENNA STRUCTURE

The two mirrored QOBFs are connected to an array of septum polarizers made of 32 elements, through a PPW bent section. The connection of all antenna parts is not trivial. In particular the input ports of the arrays of septum are separated by a metallic wall of 0.5 mm. Such a thickness cannot be used for the bottom parts of the QOBFs for mechanical constraints. Therefore a PPW 90° bend has been added at the end of QOBFs as sketched in Fig. 10. The bend has been designed following the procedure outlined in [31] and optimized to reduce reflections. A smooth transition of about λ_0 has been added to connect the PPW of the lens ($h_{\mathrm{ppw}} = 2$ mm) to the input rectangular waveguide of the septum with an height $h_t = 2.925$ mm. The array of septum polarizers is then connected between the two stacked QOBFs with the metallic wall of the septums housed in a specific slot in the lower plates of the QOBFs, as shown in the exploded wiew in Fig. 10. To guarantee the electrical contact between the components an RF choke is introduced on the lower plate of both the QOBFs.

III. MANUFACTURING AND EXPERIMENTAL RESULTS

The antenna has been manufactured in a modular way, with 5 different parts: each QOBF has been realized by milling of

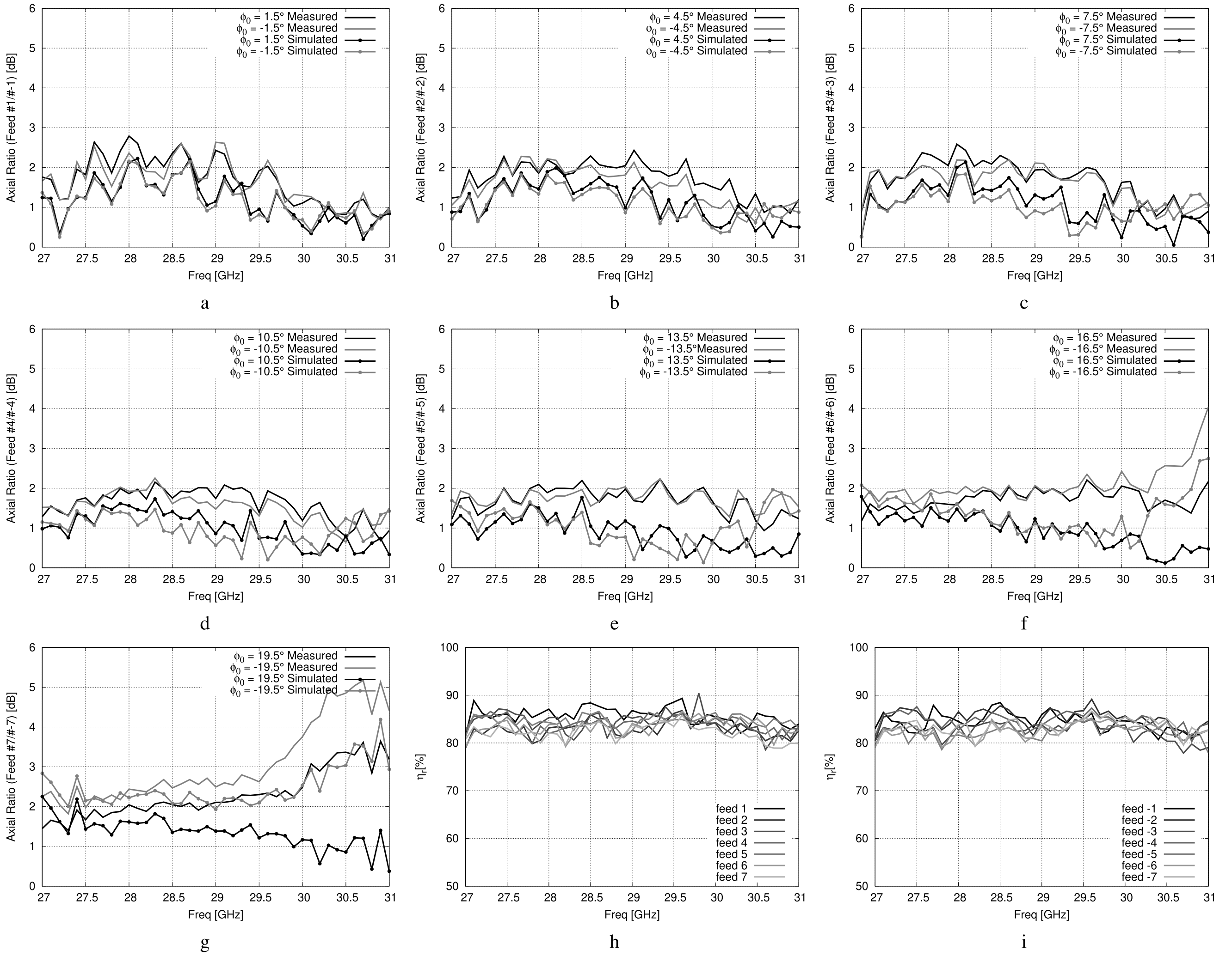

FIGURE 15. Axial ratio and efficiency of the antenna for each active feed shown in Fig. 1: (a)–(g) Measured (solid lines) and simulated (dotted lines) axial ratio, (h), measured efficiency for beams pointing in the azimuthal positive half-plane, (i) measured total efficiency for beams pointing in the azimuthal negative half-plane.

aluminium blocks, while the array of septum polarizers by EDM at IETR. The various parts are then connected by using dowel pins and screws as shown in Fig. 11. The overall size of the assembled antenna is 281.5 mm width, 245 mm length and 68.35 mm thickness. The antenna has been measured at IETR. The measured reflection coefficient, reported in Fig. 12a for each port, shows a good input matching, namely below −15 dB over the whole design bandwidth. The measured isolation between the ports, plotted in Fig. 12b, is better than −17 dB in the same band.

Fig. 13a shows the comparison between the measured radiation patterns in the azimuthal plane (the H-Plane of the antenna) at the central frequency (29 GHz) for the beam pointing at $\theta_0 = 1.5°$. In Fig. 13b, it is shown the measured normalized pattern in the elevation plane (the E-plane of the antenna). A good agreement is observed in both planes. Fig. 14 reports the measured realized gain in the H-plane for all the beams at the central frequency and at the extremes of the band. In Fig. 14a is shown that the realized gain is better than 20 dB for all the ports in almost all the operating band. In particular it can be noticed a good quality of the beams with a 3 dB beamwidth of $\theta_{3dB} = 3°$ and a low scan-loss level (better than 1.75 dB). The SLL is below −17 dB for all the beams at 27 GHz and 29 GHz, and the cross-over level is about 3 dB. At 31 GHz, the appearance of grating lobes can be observed for the extreme angles, due to the spacing of the septum array elements. Even if not reported, the cross-polar component discrimination is better than 15 dB for all the generated beams up to 29.5 GHz, beyond 29.5 GHz, for the extreme beams, it degrades as clear from the axial ratio. In Fig. 15a the comparison between the measured and simulated AR is provided for each input port. The predicted AR for the complete structure is below 2 dB for all the beams in the positive angular range while the specular beams show sightly worse performance. The AR exceeds 3 dB for the extreme beam at $\theta = 19.5°$ for frequencies above 30 GHz, for the beam at $\theta = -16.5°$ for frequencies above 30.5 GHz and above 29.5 GHz for the beam at $\theta = -19.5°$. This is due to diffraction by the surrounding structure, which was not accounted for at unit-cell level. Full-wave analyses with an infinite ground plane indicate a flatter response over frequency. The purity of the generated circular polarization is overall good, and the measured performance are in agreement with the prediction, except for the extreme beams for frequencies above 29.5 GHz where the measured AR differs from the simulated one. This may be attributed to fabrication and assembly tolerances, which have a more significant impact as diffraction effects get into play. Fig. 15h and Fig. 15h provides the measured efficiency for positive and negative scanning angles, respectively, in the azimuthal plane, when different feeds are excited. It can be observed that this antenna presents an outstanding efficiency, above 78% over the whole bandwidth in the whole scanning range. Table 3 provides a performance comparison of this contribution with recently published dual circularly-polarized antennas working in Ka-band. The table shows that the proposed antenna is bulkier with respect to planar antennas, such as the SIW array presented in [39], but it exhibits much better performance in terms of efficiency. Compared to other full-metal antennas, as the ones presented in [38] and [40], which are fixed-beam antennas, this contribution offers multi-beam capability. Moreover the proposed antenna exhibits a relative bandwidth of 8.85% in the scanning range, which is already wider than the one achieved in [38]. A fairer comparison can be made by considering only the central beams and in this case the relative bandwidth of the presented antenna is better than 20%. The presented antenna also achieves a better efficiency than the other full-metal realizations.

IV. CONCLUSION

A circularly polarized parallel plate waveguide lens-like multiple-beam antenna has been designed in the uplink of the Ka-band for SatCom applications. The antenna prototype has been manufactured completely in aluminium, adopting standard milling for the QOBFs and EDM for the septum polarizers. The antenna covers the whole uplink of the Ka-band ($27 - 31$ GHz) with a reflection coefficient and isolation between the ports below -15 dB and -18 dB, respectively. The antenna generates 14 circularly polarized beams with SLL below -17 dB, and a beamwidth of about 3° and a cross-over level between adjacent beams of about 3 dB. Moreover polarization agility is provided alternating RHCP and LHCP between adjacent beams with an axial ratio below 3 dB for a scanning range of $\pm 19°$ in the band $27 - 29.5$ GHz in measurements. Above 29.5 GHz at the extreme angles, there is the appearance of grating lobes due to manufacturing constrains. The waveguide walls thickness of 0.5 mm entails a metallization of 1 mm between two adjacent waveguides so that the spacing at 31.0 GHz is about $0.76\lambda_0$. These grating lobes in measurements appear over $\theta_0 = \pm 60°$, but it deteriorates the purity of the circular polarization. By reducing the spacing between the waveguides, it may be possible to improve the performances of this antenna in bandwidth and axial ratio. The overall size of the assembled antenna results 281.5x245x68.35mm^3. Such a size may be improved by considering multi-lens configurations. Moreover variations on the septum polarizer design allowing further compactness without sacrificing performance may be considered. In this work the choice of 7 steps septum polarizer was found necessary to provide stable response over frequency and incidence range. The proposed system presents an average efficiency of about 85%. The presented solution can only allow 1D coverage. However, 2D coverage may be achieved by stacking several lenses along the vertical direction. The rows of quasi-optical systems may be then electronically controlled to further improve the agility in scanning of the resulting antenna. Such a configuration may also increase the gain of the radiated beam. The proposed concept represents a quasi-optical sub-system, and a key building block for its 2D extensions. To the best knowledge of the authors this is the first time that such a system is fully validated experimentally, demonstrating scanning capabilities and polarization conversion and it may be considered as possible antenna solutions for Satcom applications.

ACKNOWLEDGMENT

This work has been carried out at IETR, when Nicola Bartolomei was with the University of Rennes 1. The authors would like to thank Xavier Morvan and Laurent Cronier for the fabrication of the prototype and Laurent Le Coq for performing the measurements.

REFERENCES

[1] P. Chen, W. Hong, Z. Kuai, and J. Xu, "A double layer substrate integrated waveguide Blass matrix for beamforming applications," *IEEE Microw. Wireless Compon. Lett.*, vol. 19, no. 6, pp. 374–376, Jun. 2009.

[2] J. Blass, "Multidirectional antenna—A new approach to stacked beams," in *Proc. IRE Int. Conv. Rec.*, vol. 8, Mar. 1960, pp. 48–50.

[3] N. J. G. Fonseca, "Printed S-band 4 × 4 Nolen matrix for multiple beam antenna applications," *IEEE Trans. Antennas Propag.*, vol. 57, no. 6, pp. 1673–1678, Jun. 2009.

[4] T. Djerafi, N. J. G. Fonseca, and K. Wu, "Broadband substrate integrated waveguide 4×4 Nolen matrix based on coupler delay compensation," *IEEE Trans. Microw. Theory Techn.*, vol. 59, no. 7, pp. 1740–1745, Jul. 2011.

[5] J. Butler, "Digital, matrix and intermediate-frequency scanning," in *Proc. Antennas Propag. Soc. Int. Symp.*, vol. 3, Aug. 1965, pp. 66–70.

[6] K. Tekkouk, J. Hirokawa, R. Sauleau, M. Ettorre, M. Sano, and M. Ando, "Dual-layer ridged waveguide slot array fed by a Butler matrix with sidelobe control in the 60-GHz band," *IEEE Trans. Antennas Propag.*, vol. 63, no. 9, pp. 3857–3867, Sep. 2015.

[7] C. Hua, X. Wu, N. Yang, and W. Wu, "Air-filled parallel-plate cylindrical modified Luneberg lens antenna for multiple-beam scanning at millimeter-wave frequencies," *IEEE Trans. Microw. Theory Techn.*, vol. 61, no. 1, pp. 436–443, Jan. 2013.

[8] R. C. Rudduck and C. H. Walter, "Luneberg lenses for space communications," *IRE Trans. Space Electron. Telemetry*, vol. -8, no. 1, pp. 31–38, 1962.

[9] J. Ruze, "Wide-angle metal-plate optics," *Proc. IRE*, vol. 38, no. 1, pp. 53–59, Jan. 1950.

[10] W. Rotman, "Wide-angle scanning with microwave double-layer pillboxes," *IRE Trans. Antennas Propag.*, vol. 6, no. 1, pp. 96–105, Jan. 1958.

[11] W. Rotman and R. F. Turner, "Wide-angle microwave lens for line source applications," *IEEE Trans. Antennas Propag.*, vol. AP-11, no. 6, pp. 623–632, Nov. 1963.

[12] H. Gent, "The bootlace aerial," *Royal Radar Establishment J.*, vol. 40, pp. 47–57, Oct. 1957.
[13] M. Ettorre, R. Sauleau, and L. L. Coq, "Multi-beam multi-layer leaky-wave SIW pillbox antenna for millimeter-wave applications," *IEEE Trans. Antennas Propag.*, vol. 59, no. 4, pp. 1093–1100, Apr. 2011.
[14] N. J. G. Fonseca, "Continuous parallel plate waveguide beamformer based on a bifocal constrained lens design," in *Proc. IEEE AP-S Int. Symp.*, Fajardo, Puerto Rico, Jul. 2016, pp. 1347–1348.
[15] H. Legay, "Multiple beam antenna based on a parallel plate waveguide continuous delay lens beamformer," in *Proc. Int. Symp. Antennas Propag.*, Okinawa, Japan, Oct. 2016, pp. 118–119.
[16] F. Doucet, N. J. G. Fonseca, E. Girard, H. Legay, and R. Sauleau, "Analysis and design of a continuous parallel plate waveguide multiple beam lens antenna at Ku-band," in *Proc. 11th Eur. Conf. Antennas Propag. (EUCAP)*, Mar. 2017, pp. 3631–3635.
[17] F. Doucet, N. J. G. Fonseca, E. Girard, H. Legay, and R. Sauleau, "Analytical model and study of continuous parallel plate waveguide lens-like multiple-beam antennas," *IEEE Trans. Antennas Propag.*, vol. 66, no. 9, pp. 4426–4436, Sep. 2018.
[18] F. Doucet, "Shaped continuous parallel plate delay lens with enhanced scanning performance," *IEEE Trans. Antennas Propag.*, vol. 67, no. 11, pp. 6695–6704, Nov. 2019.
[19] W. Lee, J. Kim, and Y. J. Yoon, "Compact two-layer Rotman lens-fed microstrip antenna array at 24 GHz," *IEEE Trans. Antennas Propag.*, vol. 59, no. 2, pp. 460–466, Feb. 2011.
[20] K. Tekkouk, M. Ettorre, and R. Sauleau, "SIW Rotman lens antenna with ridged delay lines and reduced footprint," *IEEE Trans. Microw. Theory Techn.*, vol. 66, no. 6, pp. 3136–3144, Jun. 2018.
[21] S. Mercader-Pellicer, W. Tang, D. Bresciani, H. Legay, N. J. G. Fonseca, and G. Goussetis, "Angularly stable linear-to-circular polarizing reflectors for multiple beam antennas," *IEEE Trans. Antennas Propag.*, vol. 69, no. 8, pp. 4380–4389, Aug. 2021.
[22] J.-C. Angevain and N. J. G. Fonseca, "Waveguide septum polarizer shaped with legendre polynomials," in *Proc. 11th Eur. Conf. Antennas Propag. (EUCAP)*, Mar. 2017, pp. 2286–2290.
[23] D. Davis, O. Digiondomenico, and J. Kempic, "A new type of circularly polarized antenna element," in *Proc. IEEE Antennas Propag. Soc. Int. Symp.*, vol. 5, Oct. 1967, pp. 26–33.
[24] N. Albertsen and P. Skov-Madsen, "A compact septum polarizer," *IEEE Trans. Microw. Theory Techn.*, vol. MTT-31, no. 8, pp. 654–660, Aug. 1983.
[25] M. Chen and G. Tsandoulas, "A wide-band square-waveguide array polarizer," *IEEE Trans. Antennas Propag.*, vol. AP-21, no. 3, pp. 389–391, May 1973.
[26] T. Ege and P. Mcandrew, "Analysis of stepped septum polarisers," *Electron. Lett.*, vol. 21, no. 24, pp. 1166–1168, Nov. 1985.
[27] J. Esteban and J. M. Rebollar, "Field theory CAD of septum OMT-polarizers," in *Proc. IEEE Antennas Propag. Soc. Int. Symp.*, vol. 4, Jun. 1992, pp. 2146–2149.
[28] J. Bornemann and V. A. Labay, "Ridge waveguide polarizer with finite and stepped-thickness septum," *IEEE Trans. Microw. Theory Techn.*, vol. 43, no. 8, pp. 1782–1787, Aug. 1995.
[29] B. Piovano, G. Bertin, L. Accatino, and M. Mongiardo, "CAD and optimization of compact wide-band septum polarizers," in *Proc. 29th Eur. Microw. Conf.*, Oct. 1999, pp. 235–238.
[30] S. V. Parekh, "Simple formulae for circular-polarization axial-ratio calculations," *IEEE Antennas Propag. Mag.*, vol. 33, no. 1, pp. 30–32, Feb. 1991.
[31] F. F. Manzillo, R. Sauleau, N. Capet, and M. Ettorre, "Mode matching analysis of an E-plane 90° bend with a square step in parallel-plate waveguide," *IEEE Antennas Wireless Propag. Lett.*, vol. 16, pp. 2187–2190, 2017.
[32] Q. Liao, N. J. G. Fonseca, and O. Quevedo-Teruel, "Compact multibeam fully metallic geodesic Luneburg lens antenna based on non-Euclidean transformation optics," *IEEE Trans. Antennas Propag.*, vol. 66, no. 12, pp. 7383–7388, Dec. 2018.
[33] N. J. G. Fonseca, A. Ali, and H. Aubert, "Cancellation of beam squint with frequency in serial beamforming network-fed linear array antennas," *IEEE Antennas Propag. Mag.*, vol. 54, no. 1, pp. 32–39, Feb. 2012.
[34] N. J. G. Fonseca, Q. Liao, and O. Quevedo-Teruel, "Equivalent planar lens ray-tracing model to design modulated geodesic lenses using non-Euclidean transformation optics," *IEEE Trans. Antennas Propag.*, vol. 68, no. 5, pp. 3410–3422, May 2020.
[35] N. J. G. Fonseca, Q. Liao, and O. Quevedo-Teruel, "Compact parallel-plate waveguide half-Luneburg geodesic lens in the Ka-band," *IET Microw., Antennas Propag.*, vol. 15, no. 2, pp. 123–130, Feb. 2021.
[36] J. P. Mahon, "Parallel plate septum polarizer for low profile antenna applications," U.S. Patent 6 861 997 B2, Mar. 1, 2005.
[37] C. D. Diallo, E. Girard, H. Legay, and R. Sauleau, "All-metal Ku-band Luneburg lens antenna based on variable parallel plate spacing fakir bed of nails," in *Proc. 11th Eur. Conf. Antennas Propag. (EUCAP)*, Mar. 2017, pp. 1401–1404.
[38] M. Ferrando-Rocher, J. I. Herranz-Herruzo, A. Valero-Nogueira, and B. Bernardo-Clemente, "Dual circularly polarized aperture array antenna in gap waveguide for high-efficiency Ka-band satellite communications," *IEEE Open J. Antennas Propag.*, vol. 1, pp. 283–289, 2020.
[39] Q. Wu, J. Hirokawa, J. Yin, C. Yu, H. Wang, and W. Hong, "Millimeter-wave multibeam endfire dual-circularly polarized antenna array for 5G wireless applications," *IEEE Trans. Antennas Propag.*, vol. 66, no. 9, pp. 4930–4935, Sep. 2018.
[40] J. Wu, Y. J. Cheng, H. B. Wang, Y. C. Zhong, D. Ma, and Y. Fan, "A wide-band dual circularly polarized full-corporate waveguide array antenna fed by triple-resonant cavities," *IEEE Trans. Antennas Propag.*, vol. 65, no. 4, pp. 2135–2139, Apr. 2017.
[41] B. Deutschmann and A. F. Jacob, "Broadband septum polarizer with triangular common port," *IEEE Trans. Microw. Theory Techn.*, vol. 68, no. 2, pp. 693–700, Dec. 2019.
[42] Z. Ding, R. Jin, S. Yang, and X. Zhu, "Design of septum polarizer waveguide feed manufactured by split-block technique," in *Proc. IEEE Int. Symp. Antennas Propag. North Amer. Radio Sci. Meeting*, Jul. 2020, pp. 1939–1940.
[43] G. Jazani and A. Pirhadi, "Design of dual-polarised (RHCP/LHCP) quad-ridged horn antenna with wideband septum polariser waveguide feed," *IET Microw., Antennas Propag.*, vol. 12, no. 9, pp. 1541–1545, Jul. 2018.
[44] A. Ludwig, "The definition of cross polarization," *IEEE Trans. Antennas Propag.*, vol. AP-21, no. 1, pp. 116–119, Jan. 1973.
[45] C. A. Balanis, *Antenna Theory: Analysis and Design*. Hoboken, NJ, USA: Wiley, 2005.
[46] F. Dubrovka, S. Piltyay, O. Sushko, R. Dubrovka, M. Lytvyn, and S. Lytvyn, "Compact X-band stepped-thickness septum polarizer," in *Proc. IEEE Ukrainian Microw. Week (UkrMW)*, Sep. 2020, pp. 135–138.
[47] C. A. Leal-Sevillano, K. B. Cooper, J. A. Ruiz-Cruz, J. R. Montejo-Garai, and J. M. Rebollar, "A 225 GHz circular polarization waveguide duplexer based on a septum orthomode transducer polarizer," *IEEE Trans. THz Sci. Technol.*, vol. 3, no. 5, pp. 573–583, 2013.
[48] Y. Hasegawa, H. Maezawa, and H. Ogawa, "Novel 500-GHz band waveguide stepped septum-type circular polarizer with a new high-accuracy and very small waveguide flange," *J. Infr., Millim., THz Waves*, vol. 42, no. 1, pp. 1–16, Jan. 2021.
[49] Y. Hasegawa, R. Harada, K. Tokuda, K. Kimura, H. Ogawa, T. Onishi, A. Nishimura, J. Han, and M. Inoue, "A new approach to suppress the effect of machining error for waveguide septum circular polarizer at 230 GHz band in radio astronomy," *J. Infr., Millim., THz Waves*, vol. 38, no. 5, pp. 638–652, May 2017.
[50] N. Bartolomei, "Circularly polarized parallel plate waveguide multiple-beam lens-like antenna for satcom applications," in *Proc. 13th Eur. Conf. Antennas Propag. (EuCAP)*, Mar. 2019, pp. 1–3.

NICOLA BARTOLOMEI received the B.Sc. and M.Sc. degrees (summa cum laude) in electronic engineering and the Ph.D. degree in telecommunication engineering from the University of Florence, in 2010, 2013, and 2017, respectively. In 2016, he was a Visiting Student with Tsinghua University, Beijing, working on travelling wave slot antennas and transmitarrays. From May 2017 to February 2020, he was with the Institut d'Electronique et des Technologies du numéRique (IETR), University of Rennes 1, Rennes, France, as a Postdoctoral Fellow in a framework founded by Thales Alenia Space, working on quasi-optical lenses for space applications. He is currently serving as an Antenna Engineer with Wave-Up S.r.l.–Innovation in Electromagnetics, Siena, Italy, involved in research and development activities on metasurface antennas. His research interests include numerical methods for scattering and antenna problems, periodic structures, metasurfaces, and slot array design.

DARWIN BLANCO received the B.Sc. degree in electrical engineering from the University of Antioquia, Medellín, Colombia, in 2009, and the M.Sc. and Ph.D. degree (summa cum laude) in multimedia and communications from the University Carlos III de Madrid, Madrid, Spain, in 2011 and 2014, respectively. He was a Postdoctoral Researcher with the University of Rennes 1, Rennes, France, from 2015 to 2016. In 2017, he worked as a Postdoctoral Researcher with the Terahertz Sensing Group, Delft University of Technology, Delft, The Netherlands. In 2019, he joined Ericsson, Sweden, where he is currently working as an Antenna and Filter Researcher. His research interests include frequency selective surfaces, RISs, filters, wideband antennas, lens antennas, and the analysis and design of unconventional phase array antennas.

FRANÇOIS DOUCET was born in Vannes, France, in 1992. He received the master's degree in engineering from the Ecole Nationale de l'Aviation Civile (ENAC), Toulouse, France, in 2015, and the Ph.D. degree in electronics from the Institut d'Electronique et de Télécommunications de Rennes, University of Rennes 1, Rennes, France, in collaboration with the European Space Research and Technology Centre, European Space Agency, Noordwijk, The Netherlands, and Thales Alenia Space, Toulouse, in 2019. For six months, he was as an Intern with the Research and Technologies Department, Thales Alenia Space, where he carried out his master's thesis project. He holds one patent. During his Ph.D. degree, he contributed to the development of parallel plate waveguide lenses for millimeter-wave multiple beam applications. In 2019, he joined Dassault Aviation, Saint-Cloud, France, as an Antenna and Radiofrequency Engineer. He was a recipient of the Robert Aladenyse ENAC Special Prize, rewarding the best end of studies internship.

ETIENNE GIRARD received the degree in electrical engineering and the Ph.D. degree from the National Institute of Applied Sciences, Rennes, France, in 2000 and 2003, respectively.

In 2003, he joined Alcatel Space (now Thales Alenia Space), Toulouse, France. He initially participated to French, European, and ESA studies in the areas of reconfigurable reflectarray through the use of MEMS. From 2007 to 2008, he worked at JayBeam Wireless, Loire Valley, developing base station antennas for wireless communications. Since 2008, he has been with Thales Alenia Space and his activities are with the Research and Technology Department on Space Antennas. He firstly developed quasi-optical beamformer antennas for a large range of Ka-band space missions and with a large variety of manufacturing process from traditional milling to injection molding. Demonstratign the first Ka-band quasi-optical beamformer in metallised injected plastic. He is currently focusing on the one hand on antenna modeling demonstrating the interest of overlapped antenna architecture and on the other hand developing high-efficiency feed, both for a very-high-throughput antenna targeting to distribute everywhere on earth a high number of very directive beams. He is an Antenna Specialist at the THALES Group. In 2022, he received the "Médaille d'honneur du travail" for 20 years of service. He co-supervised more than seven Ph.D. students. He contributed to five patents and more than 20 papers. He has experience in national, ESA, and EU projects.

HERVÉ LEGAY received the degree in electrical engineering and the Ph.D. degrees from the National Institute of Applied Sciences, Rennes, France, in 1988 and 1991, respectively. He was a Postdoctoral Fellow with the University of Manitoba, Winnipeg, MB, Canada. In 1994, he joined Alcatel Space (now Thales Alenia Space), Toulouse, France. He initially conducted studies in the areas of military telecommunication satellite antennas and antenna processing. He designed the architecture and the antijamming process of the Syracuse three active antenna. He is currently the Head of the R&T on Space Antennas, developing new antenna concepts with emerging technologies (reflectarrays, integrated antennas, multiple beam quasi-optical antennas, innovative active architectures, antenna processing, and so on). He is also the Co-Director of the joint laboratory MERLIN, involving Thales Alenia Space, and the Institut d'Electronique et de Télécommunication de Rennes, Rennes. He coordinates the collaborations with academic and research partners. He has authored 40 patents. He is the Chair of a Group of Antenna Experts at Thales Group. He was a co-prize winner of the 2007 Schelkunoff Prize Paper Award. He was a recipient of the Gold Thales Awards, in 2008, a reward for the best innovations in the Thales Group.

NELSON J. G. FONSECA (Senior Member, IEEE) received the M.Eng. degree in electrical engineering from the Ecole Nationale Supérieure d'Electrotechnique, Electronique, Informatique, Hydraulique et Télécommunications (ENSEEIHT), Toulouse, France, in 2003, the M.Sc. degree in electrical engineering from the Ecole Polytechnique de Montreal, Quebec, Canada, in 2003, and the Ph.D. degree in electrical engineering from the Institut National Polytechnique de Toulouse—Université de Toulouse, France, in 2010. He is currently working as an Antenna Engineer with the Antenna and Sub-Millimetre Waves Section, European Space Agency (ESA), Noordwijk, The Netherlands. Since November 2020, he has been holding an honorary appointment as a Professional Fellow with the University of Technology Sydney (UTS), Ultimo, NSW, Australia. He has authored or coauthored more than 270 papers in peer-reviewed journals and conferences and has over 50 patents issued or pending. His current research interests include multiple beam antennas for space missions, beam-former theory and design, ground terminal antennas, transfer of technology to and from terrestrial systems, including 5G networks, and novel manufacturing techniques. He is serving as an Associate Editor for the *IET Microwave, Antennas and Propagation* and the IEEE TRANSACTIONS ON ANTENNAS AND PROPAGATION, and a Topic Editor for the IEEE JOURNAL OF MICROWAVES. He is also serving as the Chair of the newly founded IEEE MTT-S Technical Committee 29 on Microwave Aerospace Systems. He has been a Board Member of the European School of Antennas (ESoA), since January 2019. He is actively involved both as a Lecturer and a Coordinator in courses related to space and ground antennas. He is the elected EurAAP Regional Delegate representing Benelux for the term, from 2021 to 2023. He received several prizes and awards, including the Best Young Engineer Paper Award at the 29th ESA Workshop on Antennas, in 2007, the ESA Teamwork Excellence Award, in 2020, the multiple ESA Technical Improvement Awards, and the Best Applied Technology Antenna Paper Award at EuCAP 2022.

RONAN SAULEAU (Fellow, IEEE) received the master's and M.Sc. degrees in electrical engineering and radio communications from the Institut National des Sciences Appliquées, Rennes, France, in 1995, the Agrégation degree from the Ecole Normale Supérieure de Cachan, France, in 1996, and the Ph.D. degree in signal processing and telecommunications and the Habilitation à Diriger des Recherches degree from the University of Rennes 1, France, in 1999 and 2005, respectively. He was an Assistant Professor and an Associate Professor with the University of Rennes 1, from September 2000 to November 2005, and from December 2005 to October 2009, respectively, where he has been appointed as a Full Professor, since November 2009. His current research interests include numerical modeling, millimeter-wave beam steering antennas, substrate integrated waveguide antennas, lens-based focusing devices, periodic and non-periodic structures (FSS, metasurfaces, polarizers, reflectarrays, and transmitarrays), and biological effects of millimeter waves. He has been involved in more than 70 research projects at the national and European levels and has co-supervised 27 postdoctoral fellows, 57 Ph.D. students, and 50 master's students. He has received 20 patents. He is the author or coauthor of more than 275 journal articles and 570 publications in international conferences and workshops. He was the Co-Director of the Research Department Antenna and Microwave Devices, IETR, and the Deputy Director of IETR, from 2012 to 2016. He is currently the Director of IETR. He received the 2004 ISAP Conference Young Researcher Scientist Fellowship, Japan, and the First Young Researcher Prize in Brittany, France, in 2001, for his research work on gain-enhanced Fabry-Perot antennas. In September 2007, he was elevated to a Junior Member of the Institut Universitaire de France. He was awarded the Bronze Medal by CNRS, in 2008, and the Silver Medal, in 2020. He received the 2021 Antenna EurAAP Award. He was the co-recipient of several international conference awards with some of his students (International School of BioEM 2005, BEMS'2006, MRRS'2008, E-MRS'2011, BEMS'2011, IMS'2012, Antem'2012, BioEM'2015, EuCAP'2019, EuCAP'2021, and EuMW'2022). He served as a Guest Editor for the IEEE Transactions on Antennas and Propagation with a Special Issue on "Antennas and Propagation at mm and sub mm waves." He served as a national delegate for several EU COST actions. He has served as a national delegate for EurAAP and a Member of the Board of Director for EurAAP, from 2013 to 2018.

MAURO ETTORRE (Fellow, IEEE) received the Laurea degree (summa cum laude) in electrical engineering and the Ph.D. degree in electromagnetics from the University of Siena, Italy, in 2004 and 2008, respectively. Part of his Ph.D. work was developed at the Netherlands Organisation for Applied Scientific Research (TNO), The Hague, The Netherlands, where he later worked as an Antenna Researcher. From 2008 to 2010, he was a Postdoctoral Fellow at the Institut d'Electronique et de Télécommunications de Rennes (IETR), University of Rennes 1, France. From 2010 to 2016, he was a Visiting Scholar with the Radiation Laboratory, Department of Electrical Engineering and Computer Science, University of Michigan, Ann Arbor, MI, USA. Since October 2010, he has been a Research Scientist at the Centre National de la Recherche Scientifique (CNRS), IETR. From 2014 to 2020, he assumed responsibilities for the multi-beam antenna activity for satellite applications in the joint laboratory between IETR and Thales Alenia Space, France. Since 2017, he has been serving as an Associate Editor for the IEEE Transaction on Antennas and Propagation. His research interests include the analysis and design of leaky-wave antennas, periodic structures, millimeter-wave antennas, non-diffractive radiation and localized waves, near-field focusing techniques, and wireless power transfer systems. In 2017, 2018, and 2019, he was a member of the Best Paper Award Selection Committee for the IEEE Transactions on Terahertz Science and Technology. In 2020, he co-founded the open access journal *Reviews on Electromagnetics* (European Association on Antennas and Propagation—EurAAP) for which he serves as an Associate Editor. In 2020 and 2021, he was appointed EurAAP Ambassador. He received the Young Antenna Engineer Prize at the 2008 ESA Antenna Workshop, The Netherlands; the Innovation Award at 2018 ESA Antenna Workshop, The Netherlands; the Best Paper Award in Electromagnetics and Antenna Theory at the 2018 European Conference on Antennas and Propagation (EuCAP), London, U.K.; and the Best Antennas Paper Award at EuCAP 2021, Düsseldorf, Germany.